J. Membrane Biol. 207, 169–181 (2005)
DOI: 10.1007/s00232-005-0812-1

The Journal of
Membrane
Biology

Interactions Between Charged Residues in the Transmembrane Segments of the Voltage-sensing Domain in the hERG Channel

M. Zhang[1], J. Liu[2], M. Jiang[1], D.-M. Wu[1], K. Sonawane[3], H.R. Guy[3], G.-N. Tseng[1]

[1]Department of Physiology, Virginia Commonwealth University, Richmond, VA 23298, USA
[2]Institute of Molecular Medicine, Peking University, Beijing 100871, China
[3]Laboratory of Experimental and Computational Biology, National Cancer Institute, National Institutes of Health, Bethesda, MD 20892, USA

Received: 30 July 2005/Revised: 9 October 2005

Abstract. Studies on voltage-gated K channels such as Shaker have shown that positive charges in the voltage-sensor (S4) can form salt bridges with negative charges in the surrounding transmembrane segments in a state-dependent manner, and different charge pairings can stabilize the channels in closed or open states. The goal of this study is to identify such charge interactions in the hERG channel. This knowledge can provide constraints on the spatial relationship among transmembrane segments in the channel's voltage-sensing domain, which are necessary for modeling its structure. We first study the effects of reversing S4's positive charges on channel activation. Reversing positive charges at the outer (K525D) and inner (K538D) ends of S4 markedly accelerates hERG activation, whereas reversing the 4 positive charges in between either has no effect or slows activation. We then use the 'mutant cycle analysis' to test whether D456 (outer end of S2) and D411 (inner end of S1) can pair with K525 and K538, respectively. Other positive charges predicted to be able, or unable, to interact with D456 or D411 are also included in the analysis. The results are consistent with predictions based on the distribution of these charged residues, and confirm that there is functional coupling between D456 and K525 and between D411 and K538.

Key words: Voltage-gated K channel — Structure-function relationship — Mutagenesis — Voltage clamp — *Xenopus laevis* — Oocytes

Correspondence to: G.-N. Tseng; email: gtseng@hsc.vcu.edu

Introduction

The human ether-a-go-go related gene (hERG) encodes the pore-forming component of the rapid delayed rectifier (I_{Kr}) channel [27], which is important for maintaining proper electrical activity in cardiac myocytes and in some other cell types [2, 6, 26, 29, 36, 39]. There is an intense interest in the 3-dimensional (3-D) structure of the hERG channel because it is the culprit of acquired long QT syndrome: hERG can be blocked by a wide variety of drugs, leading to prolongation of ventricular action potentials and increased risk for ventricular arrhythmia [25]. Pharmaceutical companies need to screen against compounds that can block hERG early during their drug development process. Knowledge about the 3-D structure of the hERG channel, especially the potential drug binding sites, in different gating conformations can help chemists avoid structures that are likely hERG blockers. Direct determination of hERG's 3-D structure is a remote possibility. The best available approach is to combine homology modeling of the hERG channel (based on available crystal structures of bacterial K channels [5, 11, 12, 14] and a mammalian K channel [19]) with indirect structural information deduced from functional studies of hERG with site-specific mutations.

The goal of this study is to identify interactions between charged residues in the transmembrane segments of hERG's voltage-sensing domain. The hERG channel shares the structural design with other voltage-gated K (Kv) channels (Fig. 1*A*). There are 6 positive charges in hERG's voltage-sensor (S4): K525, R528, R531, R534, R537, and K538. Previously we have shown that removing any one of the first 3 positive charges reduced the number of gating charges (estimated by the limiting slope method) transferred

during activation [38]. Furthermore, side chains at these 3 positive charge positions change their position relative to the membrane barrier during hERG activation, as was measured by changes in the accessibility of cysteine side chains introduced into these positions to external or internal thiol-modifying reagent, MTSET [38]. On the other hand, removing any one of the remaining 3 positive charges did not affect the number of gating charges transferred during channel activation, and cysteine side chains introduced into these 3 positions were accessible to intracellular MTSET, but not to extracellular MTSET, in all gating states. Positive charges in the S4 segment are not just responsible for voltage sensing and gating-charge transfer. They are also involved in stabilizing the channel in different gating conformations. This can occur by salt-bridge formation between S4's positive charges and negative charges in the neighboring transmembrane segments [23, 30, 33]. There are 6 negative charges in hERG's voltage-sensing domain: D411, D456, D460, D466, D501, and D509 (Fig. 1). Previously, we have studied the functional role of these negative charges and the sidedness of their side chains in different gating states. Substituting 5 of the 6 aspartates with cysteine (except D456C, which is not functional) markedly accelerates channel deactivation, suggesting that these negative charges serve to stabilize the hERG channel in the open state [18]. Side chains at positions 460 and 509 are accessible to the extracellular aqueous phase in all gating states, and the side chain at 466 is accessible to the extracellular phase preferentially in the closed state [18]. By inference, the 456 side chain is accessible to the outside in all gating states. The side chain at 501 is not accessible to either the extracellular or the intracellular crevice [18]. Among the negative charge positions, only 411 is accessible to the intracellular aqueous phase. The state dependence and sidedness of side chain accessibility at positive and negative charge positions in the transmembrane segments of hERG's voltage-sensing domain are depicted in the cartoons shown in Fig. 1*A*.

The motivation to undertake this study is twofold. First, this information will provide constraints on the spatial relationship among the transmembrane segments in hERG's voltage-sensing domain. This is important in the attempt to create a 3-D structural model of hERG based on homology modeling. As was discussed by Long et al. [19], although the pore domain conformations are well conserved among different K channels (consistent with their well conserved function), the conformations of the voltage-sensing domains in different Kv channels are likely to be more divergent based on the differences in their gating behavior. Therefore, information about charge interactions in the voltage-sensing domain is needed to help constrain the models. Second, this information may help us better understand the unique gating behavior of the hERG channel. Compared with most

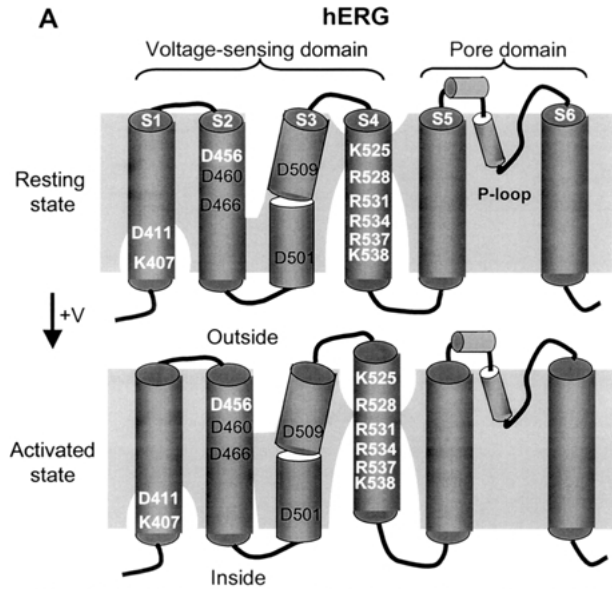

B

		Shaker	hERG	dEAG			Shaker	hERG	dEAG
S1	+0	-	K407	K236	S4	+1	R362	-	-
	-1	-	D411	D240		+2	R365	K525	K347
S2	-2	E283	D456	D274		+3	R368	R528	R350
	-3	-	D460	D278		+4	R371	R531	R353
	-4	E293	D466	D284		+5	K374	R534	R356
S3	-5	D316	D501	D319		+6	R377	R537	R359
	-6	-	D509	D327		+7	H378	K538	K360

Fig. 1. (*A*) Diagram of a hERG channel subunit that can be divided into a voltage-sensing domain (S1 – S4) and a pore domain (S5 – P-loop – S6). Negatively and positively charged residues in the transmembrane segments of the voltage-sensing domain are denoted, and those studied here are highlighted by white lettering. The subunit is embedded in a membrane lipid bilayer, with putative water-filled crevices surrounding parts of the transmembrane segments. These crevices are connected to either extracellular or intracellular aqueous phase. Upon membrane depolarization (+V), the subunit changes conformation from resting to activated states, during which the first 3 positive charges on S4 alter their positions relative to the hypothetical membrane lipid barrier that separates the extracellular and intracellular crevices around S4. D466 on S2 also changes from being exposed to an extracellular crevice to less exposed. The diagram is based on [18, 38]. (*B*) Residues and position numbers of charged residues in the voltage-sensing domains of Shaker, hERG and d(rosophila)EAG channels. Residues are denoted by generic numbers: +0 (S1), +1 to +7 (S4), and −1 to −6 (S1 – S3).

Kv channels, hERG has a relatively slow activation rate [24]. Previous studies have suggested that this is due to slow S4 movements during membrane depolarization [24, 31]. One contributing factor to such slow S4 movements in the hERG channel may be unique charge interactions in the closed state that stabilize hERG in this conformation.

In this study, we first characterize the effects of reversing the 6 positive charges in hERG's S4 segment, one at a time, on the voltage-dependence and kinetics of channel activation. This analysis suggests that K525 and K538 at the two ends of hERG's S4 may play a key role in stabilizing the channel in the

closed state. We then study which negative charges in hERG's voltage-sensing domain may interact with K525 and K538. Since none of the charge-reversal mutations in the hERG channel disrupt channel folding and trafficking, the 'intragenic rescue' approach, which has been successfully applied to studying charge pairings in the Shaker channel [23], is not applicable to the hERG channel. Therefore, we use an alternative approach, mutant cycle analysis [37], to study whether charged residues are functionally coupled in the hERG channel. Our results suggest that D411 (which is unique for the EAG family including hERG, Fig. 1*B*) can interact with K538 at the inner end of S4, while D456 (conserved among Kv channels) can interact with K525 at the outer end of S4. We discuss the structural implications of our data in the context of the 'conventional gating model' [1], instead of the more recent 'paddle gating model' [13]. The latter model has been seriously challenged by experimental findings from Shaker and other Kv channels [1, 3, 4, 7, 10, 15, 16, 32] and appears not consistent with the most recent crystal structure of a mammalian Kv1.2 channel [19, 20].

Materials and Methods

Mutagenesis

The hERG plasmid was a kind gift from Dr. Gail A. Robertson (University of Wisconsin-Madison). It was subcloned into the Kpn I/Xba I site of pAlterMax. Mutagenesis was carried out using the oligonucleotide-directed method and a commercial kit (Alter site II in vitro Mutagenesis System, Promega). Mutations were confirmed by direct DNA sequencing around the mutation sites. For transcription, plasmids were linearized by Not I and transcribed using T7 RNA polymerase, using a commercial kit (Mmessage Mmachine, Ambion, TX). The quality and quantity of cRNA products were evaluated using densitometry on RNA gels (ChemiImager model 4400, α-Innotech Corp).

Oocyte Preparation

Oocytes were isolated as described before [34] and incubated in an ND96-based medium (composition given below, supplemented with 10% horse serum and penicillin/streptomycin) at 16°C. Five to 12 h after isolation, each oocyte was injected with 40 nl of cRNA solution (containing cRNA of 4–18 ng), using a Drummond digital microdispenser. Oocytes were incubated in the above medium at 16°C, and studied 2–4 days after cRNA injection.

Voltage-clamp Experiments

Membrane currents were recorded from whole oocytes using the '2-cushion pipette' voltage clamp method [28]. During recordings, the oocyte was continuously superfused with a low-Cl ND96 solution to reduce interference from endogenous Cl channels. Voltage clamp was done at room temperature (24–26°C) with OC-725B or OC-725C amplifier (Warner Instruments, MA). Voltage-clamp protocol generation and data acquisition were controlled by pClamp5.5 via a 12-bit D/A and A/D converter (DMA, Axon Instruments, CA). Current data were low-pass filtered at 1 kHz (Frequency Devices, MA) and stored on disks for off-line analysis.

Data Analysis

Voltage-clamp protocols and methods of data analysis are described in figure legends. The following software was used for data analysis: pClamp6 or 8, EXCEL (Microsoft), SigmaPlot, SigmaStat, and PeakFit (SPSS).

The free energy involved in channel gating (ΔG_o) was calculated assuming a 2-state (closed and open) gating model [37]. Activation curves were fit with a simple Boltzmann function to estimate $V_{0.5}$ (half-maximum activation voltage) and z (equivalent gating charge). ΔG_o for channel opening at 0 mV was then calculated as $zFV_{0.5}$. In cases when the activation curve required a double-component Boltzmann function for a good fit, the $V_{0.5}$ and z values for the major component (which could be unequivocally determined, *see* D411K/R531D in Fig. 8*B* where the major Boltzmann component is the one in the more positive voltage range) were used to calculate ΔG_o. The standard error (SE) of ΔG_o was calculated as: $(Z_m^2 \cdot V_s^2 \cdot + V_m^2 \cdot Z_s^2)^{1/2}$, where z_M and z_s or V_M and V_s denote mean and SE values for z or $V_{0.5}$, respectively. Mutation-induced perturbation of free energy involved in channel gating was calculated as $\Delta\Delta G_o = \Delta G_o^{Mut} - \Delta G_o^{WT}$, where ΔG_o^{Mut} and ΔG_o^{WT} are the free energy of channel activation for mutant and WT channels, respectively. The SE value for $\Delta\Delta G_o$ was calculated as square root of the sum of the square of SE for ΔG_o values. 'Non-additivity' (or 'coupling energy') of effects of 2 mutations on the free energy of channel gating was calculated as the absolute value of '$\Delta\Delta G_o^{MUT1} + \Delta\Delta G_o^{MUT2} - \Delta\Delta G_o^{WT} - \Delta\Delta G_o^{MUT\ 1,2}$. The SE value for nonadditivity was calculated as the square root of sum of the square of SEs for the 4 $\Delta\Delta G_o$ values.

Solutions

The ND96 solution had the following composition (in mM): NaCl 96, KCl 2, $CaCl_2$ 1.8, $MgCl_2$ 1, HEPES 5, Na-pyruvate 2.5, pH 7.5. The low-Cl ND96 used during voltage-clamp experiments were made with Cl^- ions in ND96 replaced by methanesulfonate. In most experiments $[K^+]_o$ was 2 mM. In some experiments, $[K^+]_o$ was raised to 98 mM (specified in figures and Table 1). In this case, Na^+ and Na-pyruvate were omitted to maintain the osmolality.

Results

Effect of Reversing Positive Charges in hERG's S4 Segment on the Voltage Dependence and Kinetics of Channel Activation

We replace the positive charges in hERG's S4 segment with negatively charged aspartate, one at a time, and study the effects on channel gating. Figure 2 summarizes the effects on the voltage dependence of activation. Figure 2*A* depicts original current traces elicited by the voltage-clamp protocol diagrammed on top. The range of depolarization voltages (V_d, marked close to current traces) is adjusted because of mutation-induced shift in the activation curve. Figure 2*B* depicts isochronal (1 s) activation curves constructed from the relationship between V_d and the peak amplitude of tail current. These activation curves are fit with a Boltzmann

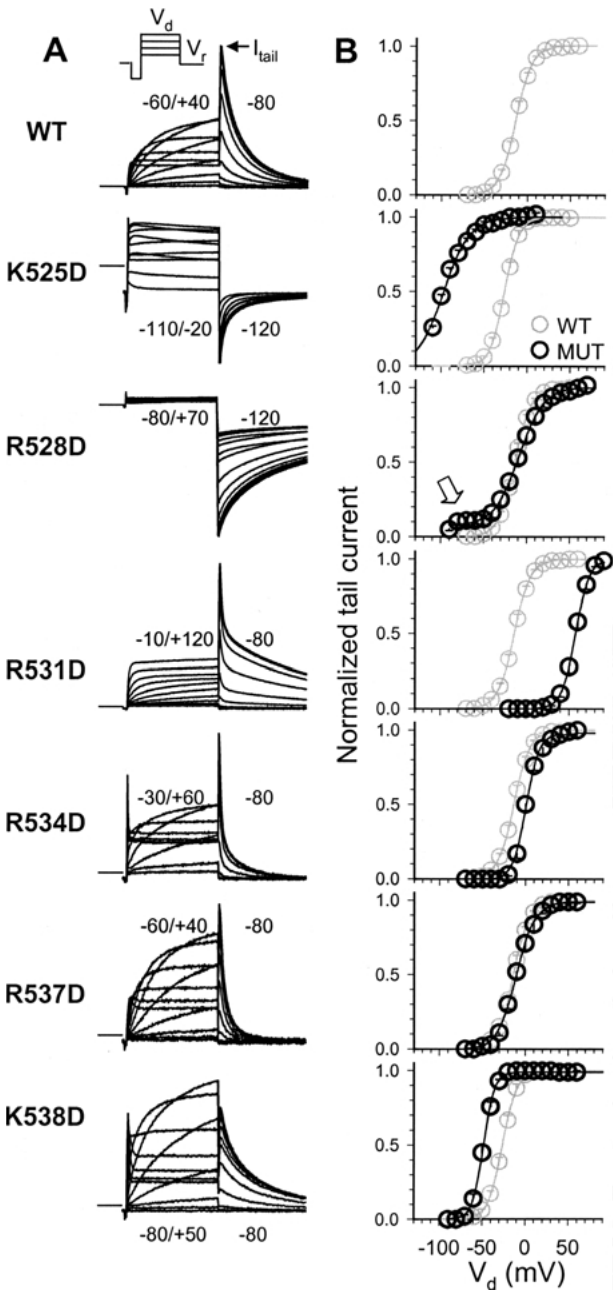

Fig. 2. Effects of substituting positively charged arginine (R) and lysine (K) in hERG's S4 with negatively charged aspartate (D) on the voltage-dependence of activation. (*A*) Original current traces from wild-type (WT) and mutant channels (specified on the left). Currents are elicited by the voltage-clamp protocol diagrammed on top: from V_h −80 mV (K525D and K538D, V_h = −120 mV), 1-s pulses to different depolarizing voltages (V_d) are applied in 10 mV increments once every 15 s (for slowly-deactivating R528D, interpulse interval = 120 s), followed by repolarization to V_r. Each depolarization pulse is preceded by a 10-ms hyperpolarizing pulse to −100 or −140 mV to evaluate the 'background' membrane conductance at V_h. For each channel, the range of V_d and V_r is marked. The horizontal lines on the left denote zero current level. (*B*) Isochronal (1-s) activation curves of WT and mutant channels (n = 3 to 10 each). For each cell, peak amplitudes of tail currents (I_{tail}, as shown in *A*) are normalized by the maximum tail current (I_{max}) after a strong V_d that fully activates the channels (ranging from 0 mV for K525D, to +120 mV for R531D). The relationship between normalized tail currents and V_d is fit with a simple Boltzmann function to estimate the half-maximum activation voltage ($V_{0.5}$) and equivalent gating charge (z): $I_{tail}/I_{max} = 1/[1+\exp((V_{0.5}-V_d)zF/RT)]$, where F, R and T are Faraday constant, gas constant and absolute temperature. To facilitate comparison, in this and Figs. 3, 4 and 6, the WT data are shown as gray symbols or gray curves in all the mutant (MUT) panels. Arrow points to a pedestal current component of R528D at negative voltages.

function to estimate half-maximum activation voltage ($V_{0.5}$) and equivalent gating charge (z). K525D and, to a smaller degree, K538D shift the activation curve in the negative direction. On the other hand, R531D and, to a smaller degree, R534D shift the activation curve in the positive direction. Although the activation curve of R528D appears similar to that of the WT channel, there is a 'pedestal' component of channel activation in the voltage range of −90 to −50 mV (*arrow* in Fig. 2*B*). This pedestal component, along with the observation that an inner cavity blocker (dofetilide) can escape from the R528D channel but not from the WT channel at hyperpolarized voltages (*data not shown*) [22], suggests that R528D has difficulty closing its activation gate at negative voltages.

We next examine the effects of mutations on the rate of channel activation. Because the fast inactivation process of the hERG channel overlaps with the activation phase, an envelope test protocol is used to estimate the rate of activation [18]. Figure 3*A* illustrates original current traces elicited by depolarization pulses to a test pulse voltage (V_t) approximately equal to the channel's $V_{0.5}$ of activation (listed on the left). Figure 3*B* summarizes τ values of activation over a wide voltage range. K525D and K538D accelerate hERG activation, while R528D and R531D have the opposite effect.

We also study the effects of mutations on the rate of channel deactivation. Figure 4*A* shows original tail current traces recorded at −80 and −120 mV. In all cases, the tail currents can be well described by a double-exponential function, generating an estimate of the fast and slow time constants of deactivation as well as the fraction of each component. The average values of τ_{Fast} and τ_{slow} of deactivation over a voltage range of −60 to −120 mV are shown in Fig. 4*B*. The distribution of the fast component of deactivation in the same voltage range is shown in Fig. 4*C*. K525D and R528D slow deactivation, R531D, R534D, and R537D accelerate deactivation, while K538D does not affect the deactivation kinetics.

The pattern of how S4 charge-reversal mutations affect the different aspects of hERG channel gating is

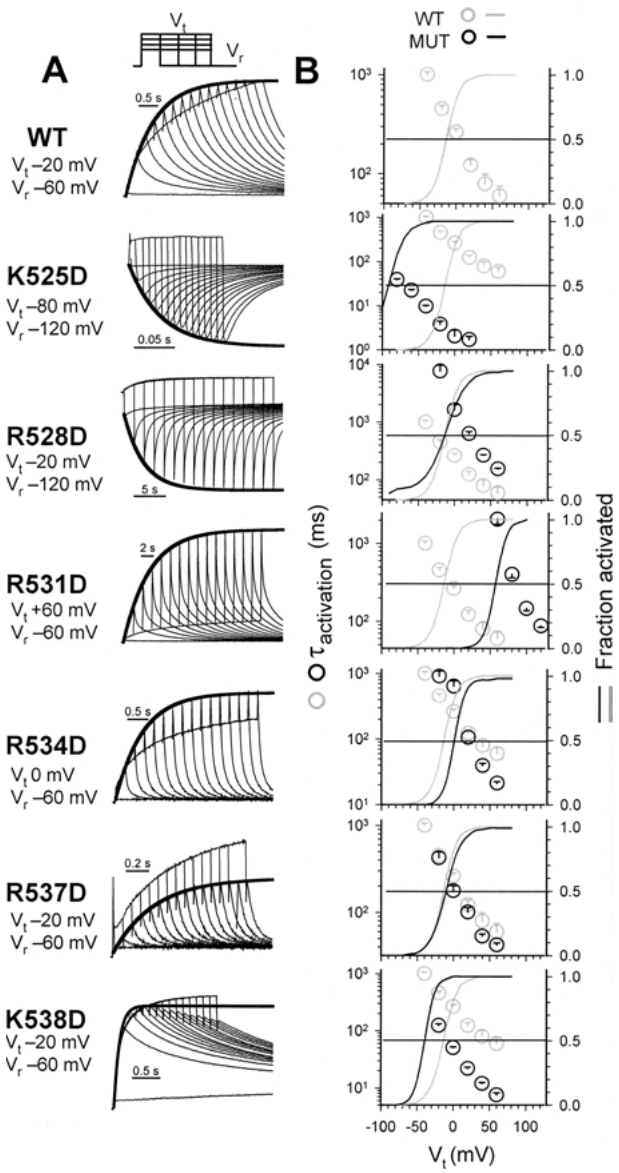

Fig. 3. Effects of substituting S4's arginine or lysine with aspartate on the kinetics of hERG activation. (*A*) Original current traces from WT and mutant channels elicited by an 'envelope test' protocol diagrammed on top: from V_h −80 or −120 mV, depolarizing pulses to V_t for various durations are applied once every 15 s (for R528D, interpulse interval = 120 s). These are followed by repolarization to V_r where the peak amplitudes of tail currents (I_{tail}) are measured. The relationship between I_{tail} and the duration of depolarizing pulse (t) can be well described by a simple exponential function with a time delay (t_{delay}): $I_{tail} = I_{max}[1-\exp(-(t-t_{delay})/\tau_{activation})]$, where $\tau_{activation}$ is time constant of activation at V_t. The superimposed thick curves represent single exponential fits to the time courses of increase in I_{tail} as the depolarizing pulses are lengthened. Note the difference in time calibrations, which is necessary due to mutation-induced acceleration or slowing of activation. For each of the channels, V_t is chosen to be close to its half-maximum activation voltage (marked to the left, along with V_r). (*B*) Values of $\tau_{activation}$ (left ordinate, logarithmic scale) are plotted against V_t. For comparison, the activation curves are also plotted (right ordinates), with a horizontal line denoting the level of half-maximum activation.

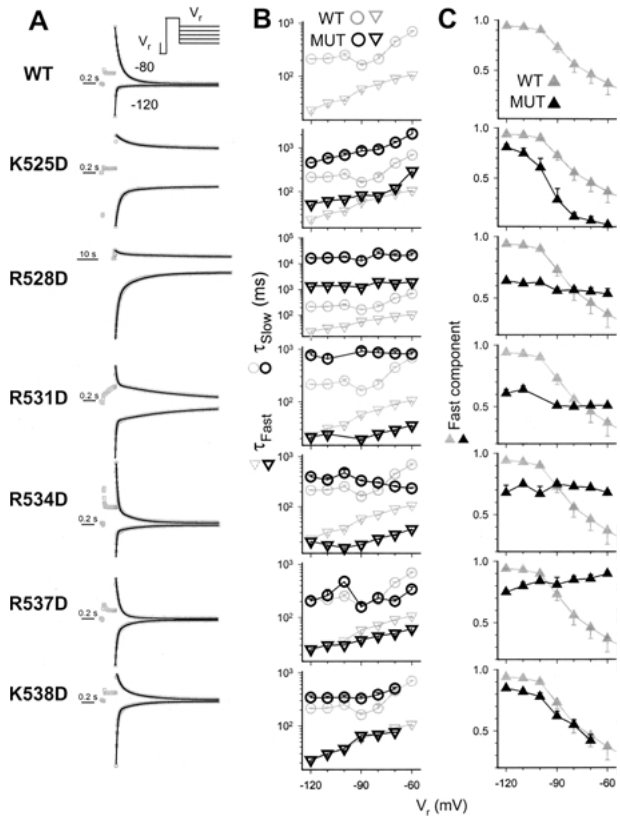

Fig. 4. Effects of substituting S4's arginine or lysine with aspartate on the kinetics of hERG deactivation. The voltage-clamp protocol is diagrammed on top of panel (*A*): from V_h −80 or −120 mV, 0.2-s depolarizing pulses to V_d at which channel activation reaches a plateau (+60 to +120 mV, based on Fig. 2*B*) are followed by repolarization to V_r ranging from −60 to −120 mV in 10 mV increments for 2 to 60 s, depending on the rate of deactivation. (*A*) Original current data points at V_r −80 and −120 mV are shown as empty gray circles. The superimposed black curves are 2-exponential fits to the tail currents: $I_{tail} = I_{Fast}\exp(-t/\tau_{Fast}) + I_{Slow}\exp(-t/\tau_{Slow})$, where τ_{Fast} and τ_{Slow} are the fast and slow time constants of deactivation, I_{Fast} and I_{Slow} are the amplitudes of respective components. (*B*) Values of τ_{Fast} and τ_{slow} are plotted against V_r on a semilogarithmic scale. (*C*) The fraction of the fast component of deactivation, $I_{Fast}/(I_{Fast} + I_{Slow})$, is plotted against V_r.

summarized in Fig. 5*A*. The pattern is clear: reversing positive charges at the two ends of S4 (K525D and K538D) reduces the free energy needed for channel activation (destabilizes closed states relative to activated states), accelerates activation and, for K525D, slows deactivation. Charge reversal at the two middle positions of S4 (R531D and R534D) increases the free energy needed for channel activation (destabilizes activated states relative to closed states), accelerates deactivation, and for R531D, slows activation. Although R528D appears to have little effect on the calculated free energy for channel activation, this mutation exhibits the most dramatic effects on the channel gating kinetics: the rate of activation is slowed by ~20 fold, and the rate of deactivation is slowed by ~40 fold.

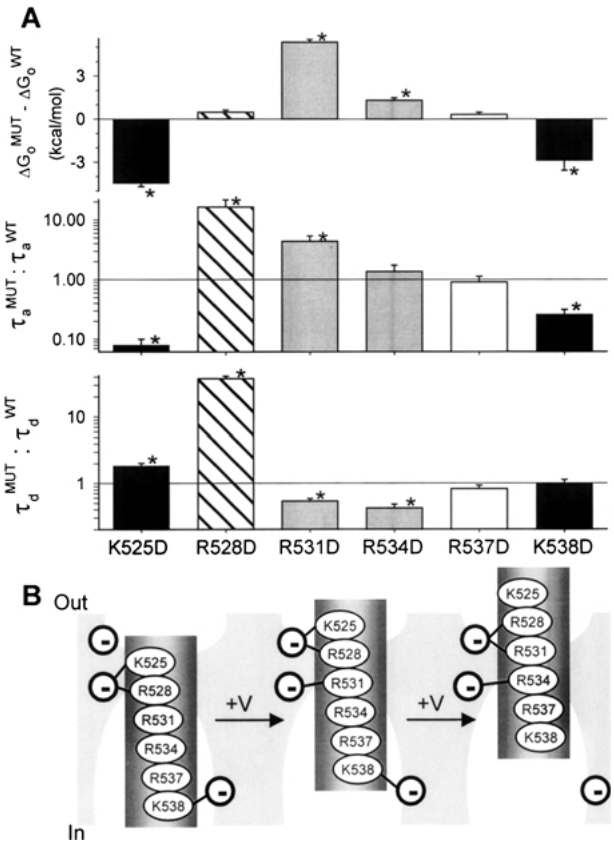

Fig. 5. Summary of charge-reversal mutations in hERG's S4 segment on channel function. (*A*) *Top:* Effects of mutations on the free energy of channel activation at 0 mV (ΔG_o) calculated based on a 2-state channel gating scheme: $\Delta G_o = zFV_{0.5}$, where z and $V_{0.5}$ are from the Boltzmann fit of the activation curve, as shown in Fig. 2*B*, and F is the Faraday constant. *Middle:* Effects of mutations on the time constant of activation (τ_a). For each channel, τ_a is measured at a V_t close to its $V_{0.5}$ of activation (as shown in Fig. 3*A*). *Bottom:* Effects of mutations on the fast time constant of deactivation (τ_d) at −120 mV as shown in Fig. 4*B*. For both middle and bottom panels, the values are normalized by those of the WT channel and shown on a logarithmic scale. *: $p < 0.05$ vs WT. (*B*) Working model to account for the observed effects of S4 charge reversal mutations on hERG gating function. S4 is diagrammed as a cylinder with positively charged residues on its surface. It is situated in a gating canal with most of its surface exposed to extracellular or intracellular aqueous crevice. Negative charges lining both crevices and in the membrane lipid bilayer can form salt bridges with S4's positive charges. Membrane depolarization (+V) causes the S4 cylinder to move in the outward direction relative to its surrounding.

Based on these findings, we propose a working model to explain the differential effects of S4 charge reversal mutations on hERG's gating function (Fig. 5*B*). Upon membrane depolarization, S4 moves in the outward direction relative to its surroundings. Positive charges on S4 pair with negative charges in the neighboring channel domains in a state-dependent manner. We suggest that K525 and K538 at the 2 ends of S4 pair with negative charges in closed states (*left* and *middle*) to stabilize these conformations. Therefore, reversing these charges destabilizes the closed states, leading to a negative shift in the activation curve, acceleration of activation and (for K525D) slowing of deactivation. On the other hand, R531 and R534 pair with negative charges mainly in the open state (*right*), and reversing these positive charges creates the opposite phenotype. R528 is the middle one of 3 positive charges involved in gating-charge transfer during hERG activation and deactivation [38]. Thus, it may play a pivotal role in determining the rate of S4's forward and backward movements. We suggest that R528 can pair with negative charges in all states. Reversing this positive charge destabilizes all the gating conformations, leading to a marked slowing of both activation and deactivation.

However, the quasi-steady state activation curve of R528D does not differ much from that of the WT channel, possibly because the destabilizing effects on different gating states cancel each other out. However, the pedestal current component (Fig. 2*B*) reveals that a fraction of the R528D channels has difficulty closing the activation gate at negative voltages.

Where are the negative charges that can pair with these S4 positive charges in a state-dependent manner? Our focus here is to identify negative charges that can pair with K525 and K538 at the two ends of S4. The diagram in Fig. 1*A* summarizes the state dependence of side chain accessibility at positive charge and negative charge positions to extracellular and intracellular aqueous phases [18, 38]. According to this diagram, D411 can potentially interact with K538, and D456 is one of several negative charges that can potentially interact with K525 as well as R528. We use the mutant cycle analysis to test whether side chains at these positions are functionally coupled. To test the power of the mutant cycle analysis in distinguishing between interacting and non-interacting charged residues, we also create S4 mutations that are predicted not to interact with D411 (R531) or D456 (R534). Finally, there is a lysine residue (K407) on the same face of S1 as D411. As shown in Fig. 1*A*, by inference the side chain at 407 is accessible to the intracellular aqueous phase. This lysine may form a salt bridge with the aspartate side chain at 411 and influence the stability of channel conformations. Therefore, we also include K407 in the mutant cycle analysis.

Effects of Charge Reversal Mutations at 411, 407 and 456 on hERG Channel Gating

Figure 6 shows that both D411K and D456R cause a marked positive shift and a decrease in the steepness of the activation curve. They also accelerate channel deactivation. However, D411K accel-

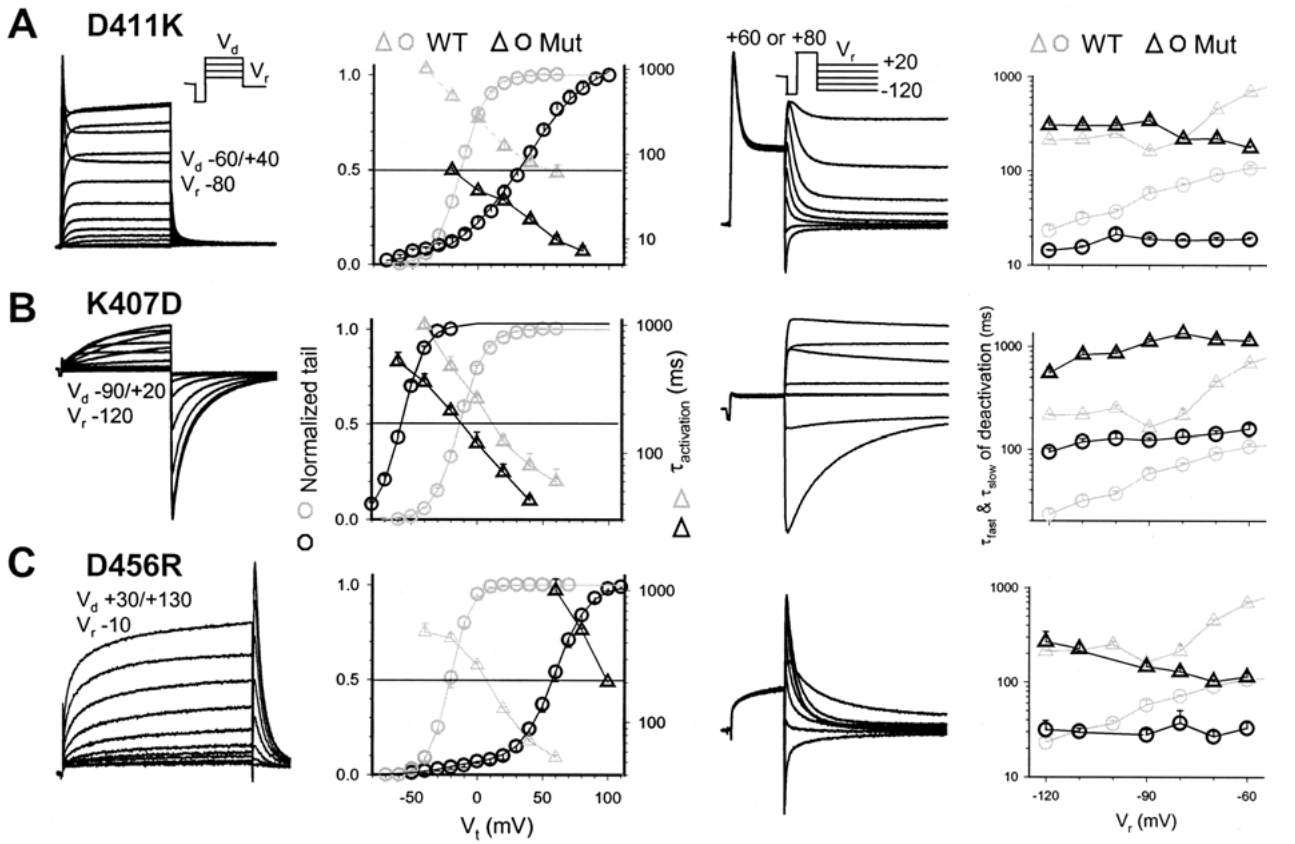

Fig. 6. Effects of charge-reversal mutations at 411 (D411K, A), 407 (K407D, B), and 456 (D456R, C) on hERG channel function. For each channel, from left to right, the first panel shows original current traces elicited by the voltage-clamp protocol diagrammed on top (for all 3 channels the duration of V_d pulse = 1 s). The second panel depicts isochronal (1-s) activation curves calculated as described for Fig. 2*B* (denoted by circles, based on left ordinate), and time constants of activation as described for 3*B* (denoted by triangles, based on right ordinate of logarithmic scale). The third panel depicts original current traces elicited by the voltage-clamp protocol diagrammed on top. The tail currents are fit with a double-exponential function as described for Fig. 4*B*. The fast and slow time constants of deactivation (τ_{Fast} circles, and τ_{Slow}, triangles) are plotted in the fourth panel against V_r. All recordings are made in $[K]_o$ 2 mM, except the τ values of activation for D456R (98 mM $[K]_o$, the WT data are also obtained in 98 mM $[K]_o$ for comparison).

erates activation (τ measured at $V_{0.5}$ of activation is 17 ± 2 ms for D41IK at +40 mV, 25-fold faster than that of the WT channel measured at −20 mV, 474 ± 85 ms), while D456R slows activation (τ measured at +60 mV is 995 ± 228 ms, 2.3-fold slower than that of the WT channel measured at −20 mV). K407D shifts the activation curve in the negative direction, slows deactivation, but has little effect on the rate of activation. These data suggest that in the WT channel, D456 is mainly involved in stabilizing the open state and K407 is involved in stabilizing closed states. D411K accelerates both activation and deactivation. This apparent contradiction suggests that D411 may be involved in stabilizing multiple gating states, a possibility supported by the observations that while D411K shifts the activation curve in the positive direction, D411C shifts the activation curve in the negative direction [18].

Using Mutant Cycle Analysis to Probe Interactions Between Charged Residues in the Transmembrane Segments of hERG's Voltage-Sensing Domain

To deduce whether there is an interaction between D456 and positive charges of S4 (K525, R528, and R534), single and double charge reversal mutations (D456R/K525D, D456R/R528D, and D456R/R534D) are studied. Since some mutant channels are expressed at a low level, we elevate $[K]_o$ to 98 mM to boost the current amplitudes ($[K]_o$ marked in Figs. 7 and 8, and in Table 1). For mutant cycle analysis, we maintain the same $[K]_o$ when recording from all 4 channels within a cycle to avoid possible confounding factors due to changes in $[K]_o$. The only exception is R528D. To observe currents through the double mutant channel (D456R/R528D), $[K]_o$ is elevated to 98 mM. The same $[K]_o$ is used for WT and D456R.

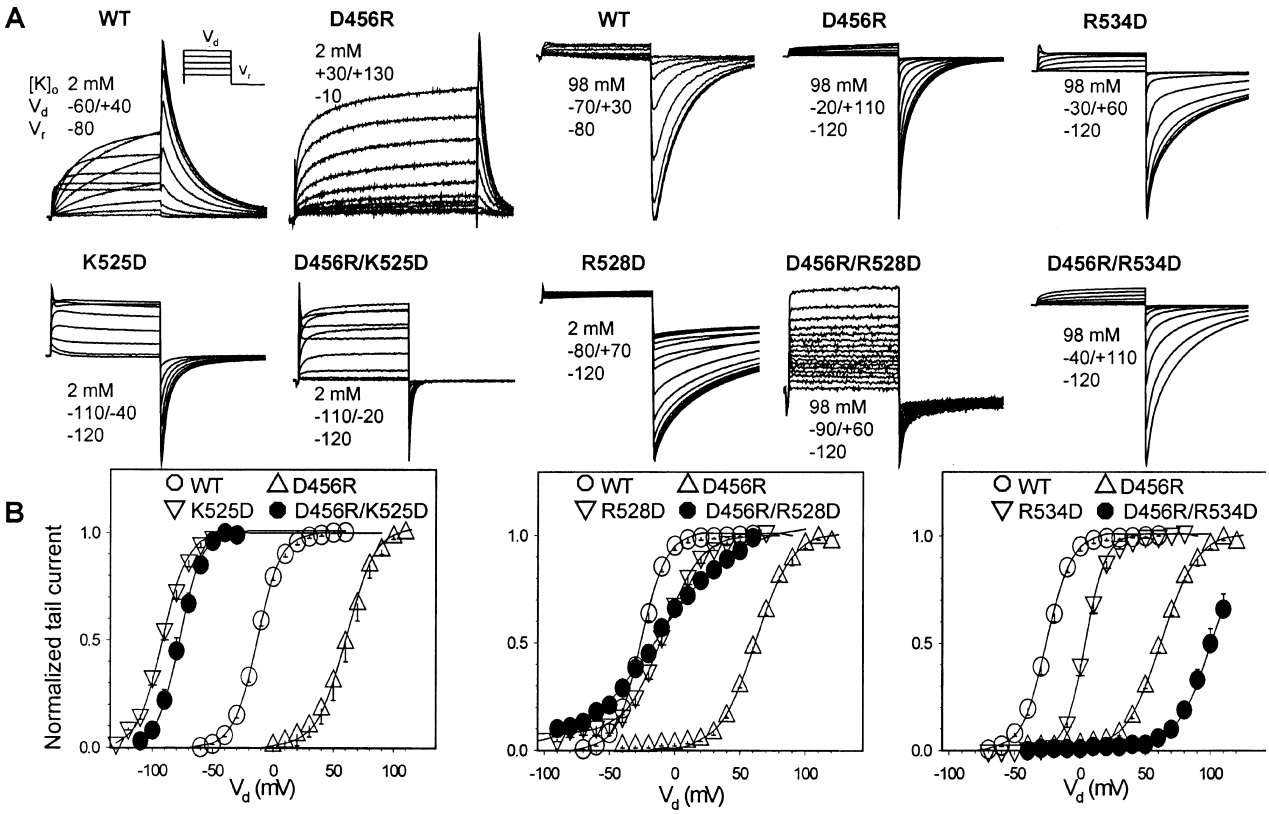

Fig. 7. Effects of single and double charge-reversal mutations of D456, K525, R528, and R534 on the voltage-dependence of hERG activation. (*A*) Original current traces elicited by the voltage-clamp protocol diagrammed in the WT panel (V_d lasts 1 s for all channels). The $[K]_o$ used during recordings, range of V_d and value of V_r are marked close to current traces. (*B*) Activation curves of WT and mutant channels.

However, the R528D single mutant cannot sustain such a high $[K]_o$. This is likely due to the constitutively active channel component at V_h, making it difficult to maintain voltage control in 98 mM $[K]_o$. Table 1 shows that elevating $[K]_o$ from 2 to 98 mM reduces ΔG_o by 0.83, 0.92 and 0.27 kcal/mol for WT, D411K, and D456R, respectively. This indicates that elevating $[K]_o$ favors the equilibrium of hERG channels toward the open state. To correct for this $[K]_o$ effect when calculating the nonadditivity value for the D456R-R528D pair, we assume that elevating $[K]_o$ induces a similar reduction in the ΔG_o value of R528D. Therefore, the ΔG_o value for R528D obtained in 2 mM $[K]_o$ is lowered by 0.55 kcal/mol (the average of ΔG_o reduction in WT and D456R, Table 1) as an estimate for ΔG_o in 98 mM $[K]_o$. Note that without this correction, the nonadditivity value for the D456R-R528D pair would be 4.15 ± 0.27 kcal/mol, which is even more dramatic than the value listed in Table 1 and will not alter our conclusion. Figure 7*A* depicts current traces from WT, single, and double mutant channels. Figure 7*B* compares the activation curves of each group of 4 channels for a mutant cycle analysis. Numerical data are listed in Table 1. For both D456R/K525D and D456R/R528D, the double mutants' activation curves are very similar to those of K525D and R528D single mutants, respectively. This suggests that the effects of D456R on hERG gating are negated by the second site mutation. On the other hand, the D456R/R534D double mutant shifts the activation curve to a very positive voltage range. The degree of shift is roughly the same as the sum of positive shifts caused by the two individual mutations.

To deduce whether there is an interaction between D411, K538, and K407 or R531, we construct activation curves for single and double charge-reversal mutations. Data are summarized in Fig. 8 and Table 1. The D411K/K407D double mutant has an activation curve largely superimposible with that of the K407D single mutant. D411K/K538D shifts the activation curve to an even more negative voltage range than that of K538D alone. Therefore, the effects of D411K on hERG gating are negated by the second site mutation. On the other hand, the changes in the activation curve of the D411K/R531D double mutant suggest that they are the sum of effects of the two single site mutations. Note that the parameter values related to the D411K/R531D double mutant ($V_{0.5}$, z, ΔG_o, $\Delta\Delta G_o$, and nonadditivity, Table 1) are all calculated

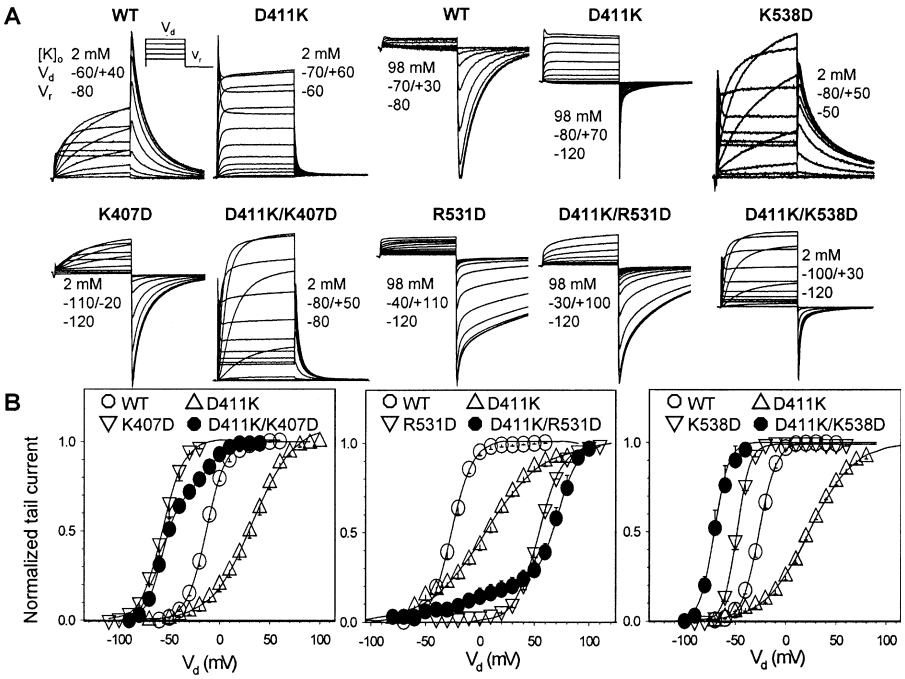

Fig. 8. Effects of single and double charge reversal mutations of D411, K407, R531, and K538 on the voltage-dependence of hERG activation. The format of this figure is the same as that of Fig. 7.

Table 1. Effects of single and double charge reversal mutations on activation gating of the hERG channel.

	$[K]_o$ (mM)	$V_{0.5}$(mV)	z	(n)	ΔG_o(kcal/mol)	$\Delta\Delta G_o$(kcal/mol)	Nonadditivity (kcal/mol)
WT	2	−13.27 ± 1.02	2.62 ± 0.08	(9)	−0.82 ± 0.07		
WT	98	−25.77 ± 1.29	2.70 ± 0.18	(5)	−1.65 ± 0.14		
D411K	2	+34.96 ± 2.15	1.27 ± 0.04	(13)	1.05 ± 0.07	1.88 ± 0.10	
D411K	98	+6.06 ± 2.48	0.89 ± 0.05	(4)	0.13 ± 0.05	1.78 ± 0.15	
K407D	2	−56.35 ± 3.14	2.74 ± 0.09	(9)	−3.66 ± 0.24	−2.83 ± 0.25	
D456R	2	+60.89 ± 4.12	2.07 ± 0.08	(6)	2.98 ± 0.23	3.81 ± 0.24	
D456R	98	+62.14 ± 1.47	1.84 ± 0.12	(5)	2.71 ± 0.19	4.36 ± 0.23	
K525D	2	−91.61 ± 2.26	2.46 ± 0.08	(10)	−5.34 ± 0.22	−4.51 ± 0.23	
R528D	2*	−8.72 ± 2.75	1.92 ± 0.09	(7)	−0.40 ± 0.13	0.43 ± 0.14	
R531D	98	+54.22 ± 1.23	2.29 ± 0.14	(3)	2.94 ± 0.19	4.59 ± 0.24	
R534D	98	+3.80 ± 1.75	3.31 ± 0.12	(3)	0.30 ± 0.14	1.95 ± 0.19	
K538D	2	−39.55 ± 1.81	4.03 ± 0.70	(4)	−3.77 ± 0.68	−2.95 ± 0.68	
D411K/K407D	2	−53.59 ± 1.41	5.55 ± 0.21	(8)	−7.04 ± 0.32	−6.22 ± 0.33	5.26 ± 0.43
D411K/R531D	98	+72.06 ± 3.33	3.02 ± 0.51	(4)	5.15 ± 0.90	6.80 ± 0.91	0.44 ± 0.93
D411K/K538D	2	−67.57 ± 3.61	4.21 ± 0.20	(6)	−6.74 ± 0.48	−5.91 ± 0.48	4.84 ± 0.84
D456R/K525D	2	−77.41 ± 2.35	2.72 ± 0.12	(5)	−4.99 ± 0.27	−4.16 ± 0.28	3.46 ± 0.42
D456R/R528D	98	−9.07 ± 3.34	0.89 ± 0.03	(5)	−0.19 ± 0.07	1.46 ± 0.15	3.60 ± 0.27*
D456R/R534D	98	+101.22 ± 3.80	1.96 ± 0.16	(5)	4.70 ± 0.42	6.35 ± 0.44	0.04 ± 0.50

The voltage-clamp protocol and data analysis are as described for Figs. 2*B* and 6–8. $[K]_o$ used during data collection is denoted. For mutant cycle analysis (Fig. 9), the same $[K]_o$ is used for all 4 channels in a mutant cycle (*except R528D in the D456R/R528D cycle, *see* text for details). $V_{0.5}$. and z refer to the half-maximum activation voltage and equivalent gating charge obtained from Boltzmann fit. ΔG_o (free energy of channel activation at 0 mV) is calculated as $zFV_{0.5}$, where F is the Faraday constant. Mutation-induced changes in ΔG_o ($\Delta\Delta G_o$) are calculated as: $\Delta G_o^{MUT} - \Delta G_o^{WT}$, where ΔG_o^{WT} and ΔG_o^{MUT} refer to ΔG_o values of WT and mutant channels. The value of non-additivity of effects of mutations at 2 locations (MUT1/MUT2) is calculated as: $[(\Delta G_o^{MUT1} - \Delta G_o^{WT}) - (\Delta G_o^{MUT1,2} - \Delta G_o^{MUT2})]$. The absolute values of nonadditivity are reported here.

based on the major Boltzmann component in the more positive voltage range.

Double mutant cycle analysis is a formal way of quantifying the degree of coupling of mutations' effects on channel function [9, 37]. In our case, the degree of non-additivity (or coupling energy) is calculated based on the free energy of channel activation. If the effects of 2 mutations on channel activation are not additive, the two mutation sites may be coupled. What is an appropriate threshold level of non-additivity based on which to judge whether the mutational effects are coupled or not? In previous studies, a non-additivity of 1 kcal/mol has served as a good cut-off value [9, 37]. Figure 9 shows that in our analysis there is a clear segregation of non-additivity values, those that are > 3 kcal/mol (D456R-K525D,

D456R-R528D, D411K-K538D, and D411K-K407D) and those that are < 1 kcal/mol (D456R-R534D and D411K-R53 ID). Therefore, we conclude that each of the mutation pairs in the first group is coupled, and those in the second group are not.

Discussion

Technical Considerations

We use a simplified 2-state gating model to evaluate the effects of charge reversal mutations on the energetics of hERG channel activation. In reality, the gating scheme should be much more complicated than the 2-state model [21, 24, 35]. Although the absolute values of calculated free energy of channel gating may not carry much physical meaning, it is the relative values that allow us to compare how easy or how difficult channels can be opened by membrane depolarization. Therefore, this approach has been commonly used in deducing the pattern of mutational effects on the energetics of channel gating [8, 17, 37]. In a previous study on pore-domain mutations in the Shaker channel, it was found that mutation-induced shift in $V_{0.5}$ value and change in z value was correlated: a more positive $V_{0.5}$ value was accompanied by a smaller z value [37]. It was further shown, by a kinetic model simulation, that this was consistent with a scenario in which most of these pore-domain mutations mainly affected a concerted conformational change between a permissive state (all 4 voltage sensors reached an activated state) and the final open state [37]. Our limited data set does not show such a correlation between $V_{0.5}$ and z values (Table 1).

Although the double mutant cycle analysis allows us to determine whether mutations at two sites are functionally coupled or not, functional coupling does not necessarily mean that the two sites are in close proximity in 3-D space. Indeed, in the study designed to examine coupling between mutations in the Shaker channel's pore-domain, almost all gating-sensitive mutations (that markedly alter the voltage-dependence of Shaker activation) were functionally coupled, although some of them are as far as 15 Å apart (based on mapping of Shaker residues to the KcsA crystal structure) [37]. On the other hand, there was no coupling between voltage-sensitive and voltage-insensitive mutations. Therefore, these findings raise questions as to whether functional coupling, as is suggested by the mutant cycle analysis, can be used to infer physical interaction in 3-D space. We believe our mutant cycle analysis reveals the likelihood of salt-bridge formation between functionally coupled residues for the following reasons. First, in our study, all charge reversal mutations are gating-sensitive, i.e., they all have marked effects on hERG gating. However, the mutant cycle analysis can clearly segregate those mutations that are coupled from those that are not coupled. Second, the pattern of residues that are coupled and those that are not coupled is consistent with predictions based on experimentally determined side-chain accessibility to extracellular or intracellular aqueous crevices (Fig. 1*A*) [18, 38]. Finally, for charged residues facing the same aqueous crevice, the confinement by the lipid surrounding is expected to accentuate charge-charge interactions and facilitate salt-bridge formation between opposite charges.

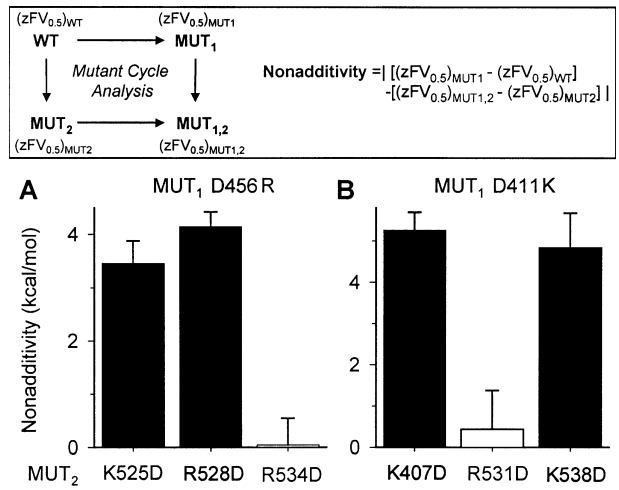

Fig. 9. *Top:* Diagram illustrating the calculation of non-additivity of mutational effects on the free energy of channel activation at 0 mV (ΔG_o). Shown on the 4 corners are WT channel, mutant channels where the first or second position is mutated (MUT_1 or MUT_2), or when both positions are mutated ($MUT_{1,2}$). The calculation of ΔG_o values is also noted. Non-additivity is calculated as the absolute value of difference between MUT_1's effect on ΔG_o tested on the WT background vs that tested on the MUT_2 background. *Bottom:* Comparison of non-additivity of charge reversal mutations, with MUT_1 marked on top (D456R in A and D411K in B), and MUT_2 listed along the abscissa.

We would like to point out that charge reversal mutations add a layer of complexity that makes the data more difficult to interpret. Unlike charge neutralization mutations that simply eliminate the effects of specific charges, charge reversal mutations may potentially introduce new interactions independent of the restoration of native charge-pairing in the WT channel. We chose to use charge-reversal mutations in this study because preliminary experiments suggested that charge reversal was more effective than charge neutralization in perturbing channel gating, thus enhancing the power of mutant cycle analysis to distinguish between coupled and uncoupled mutations.

Mechanism for the Effects of Single and Double Charge-Reversal Mutations on hERG Gating and Structural Implications

Figure 10 provides structural implications of our findings reported here and previously [18, 38] in the

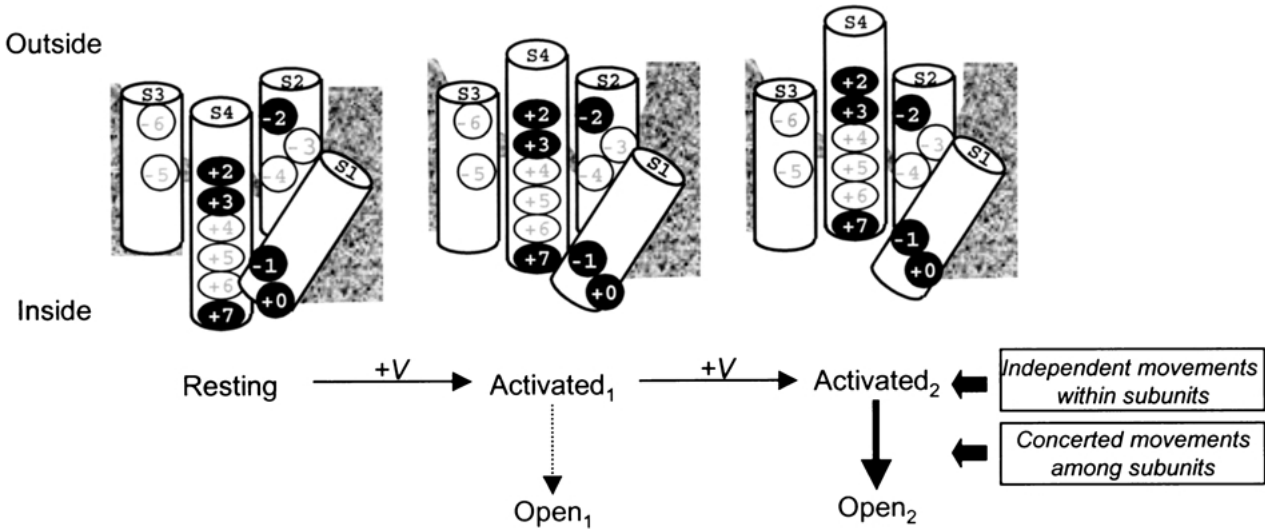

Fig. 10. Diagrams of proposed charge pairings in the hERG channel. S1 – S4 are represented by cylinders, and charged residues are denoted by generic numbers as shown in Fig. 1*B*. Those charged residues examined by double mutant cycle analysis are highlighted by white letterings in back ovals. The membrane barrier is depicted by a gray textured background, with extracellular and intracellular crevices around S1–S4 indicated (based on [18] and [38]). The channel gating states are denoted below the diagram: membrane depolarization (+V) triggers outward S4 movements in a stepwise manner so that the channel goes from resting state to early activated state ($activated_1$), and then late activated state ($activated_2$). S4 outward movements are independent conformational changes within each subunit. From the activated states, the channel can go through concerted conformational changes and open the pore. Normal channel opening preferably occurs from the late activated state (*thick vertical arrow*) rather than from the early activated state (*dotted vertical arrow*). However, when charge reversal mutations strongly stabilize the early-activated state and/or strongly destabilize the late activated state, channel opening can occur mainly from the former state.

context of the conventional gating model [1, 3, 4, 7, 10, 15, 16, 32]. S1 to S4 are depicted as transmembrane helices. Upon membrane depolarization, S4 moves in the outward direction in a stepwise manner relative to S1–S3, allowing the positive charges along S4 to pair with different negative charges in the other helices. In the resting state there is a separation between negative charges ('−2', '−3', '−4', '−5' and '−6', accessible to the extracellular aqueous phase) and positive charges ('+3', '+4', '+5', '+6' and '+7', accessible to the intracellular aqueous phase) [18, 38]. In the late activated states ($activated_2$ in Fig. 10), '+2' moves out into the extracellular aqueous phase, becoming accessible to extracellular MTSET [38]. There is considerable overlap between positive charges in the middle of S4 ('+3', '+4' and '+5') and negative charges on S2 and S3 ('−2', '−3', '−4', '−5' and '−6'), allowing charge pairings to stabilize the hERG channel in the activated state. This can explain why neutralizing or reversing the middle positive charges in S4 (replacing R528, R531 or R534 with cysteine or aspartate) can cause different degrees of hindrance to channel opening [38]. This can also explain why neutralizing any one of the negative charges (D460C, D466C, D501C, and D509C) can destabilize the open state [18].

We propose that pairing between D456 and K525 occurs early during the activation transitions ($activated_1$ in Fig. 10). D456 then pairs with R528 and R531 as S4 moves further outward to reach the late activated state, with K525 facing the extracellular aqueous phase. This scenario is consistent with the recently published crystal structure of the mammalian Kv1.2 channel in the open state: R297 (equivalent to hERG's K525, [38]) is out facing the extracellular phase, with R300 and R303 (equivalent to hERG's R528 and R531) making contact with E226 (equivalent to hERG's D456) [20]. Such a scenario can explain why K525D and D456R shift the activation curve in opposite directions. K525 pairs with negative charges (possibly D466 and D501 or '−4' and '−5' in Fig. 10) in the resting state and with D456 in the early-activated state, but moves into the extracellular aqueous space in the late activated state. Therefore, the main effect of reversing this positive charge is to destabilize the closed and early activated states, shifting the activation curve in the negative direction and accelerating channel opening. On the other hand, reversing the negative charge at 456 will also disrupt the interaction with R528 and R531 in the late activated state. This destabilizing effect outweighs the destabilizing effect on the early activated state, thus shifting the activation curve in the positive direction and slows channel opening. Why does the double mutant, D456R/K525D, favor the open state and shift the activation curve in the negative direction? We propose that while in WT hERG, channel opening preferably occurs from the late activated

state ('Activated$_2$' in Fig. 10), in the D456R/K525D mutant channel opening occurs at the earlier stage of 456R-525D pairing (Activated$_1$). This is because further S4 outward movement is prohibited by the high energy cost to break the 456R-525D salt bridge and to force R528 to approach 456R.

Our data suggest that D411 may interact with K407 and K538 at the intracellular surface of the membrane. The scenario in Fig. 10 has D411 interact with K407 in all gating states. This is reasonable because these two side chains are on the same face of the S1 helix, one helical turn apart (~ 5 Å). D411 may pair with K538 in the early activated state (Activated$_1$). This can explain why charge reversal mutations at these 2 positions (K538D and D411K) share the phenotype of accelerated activation. The double mutant, D411K/K538D, shifts the activation curve to an even more negative voltage range than that caused by K538D alone. It is possible that with simultaneous charge reversal at these two interacting sites, the channel can open from the early activated state when 411K-538D pairing occurs.

This work was supported by HL 46451 & HL 67840 from NIH/NHLBI and a grant-in-aid award from AHA/Mid-Atlantic Affiliate (GNT).

References

1. Ahern, C.A., Horn, R. 2004. Specificity of charge-carrying residues in the voltage sensor of potassium channels. *J. Gen. Physiol.* **123:**205–216
2. Bauer, C.K. Wulfsen, I., Schafer, R., Glassmeier, G., Wimmers, S., Flitsch, J., Ludecke, D.K., Schwarz, J.R. 2003. HERG K^+ currents in human prolactin-secreting adenoma cells. Pfluegers Arch. **445:**589–600
3. Broomand, A., Mannikko, R., Larsson, H.P., Elinder, F. 2003. Molecular movement of the voltage sensor in a K channel. *J. Gen. Physiol.* **122:**741–748
4. Cohen, B. E., Grabe, M., Jan, L.Y. 2003. Answers and questions from the KvAP structures. *Neuron* **39:**395–400
5. Doyle, D. A., Cabral, J.M., Pfuetzner, R.A., Kuo, A., Gulbis, J.M., Cohen, S.L., Chait, B.T., MacKinnon, R. 1998. The structure of the potassium channel: molecular basis of K^+ conduction and selectivity. *Science* **280:**69–77
6. Faravelli, L., Arcangeli, A., Olivotto, M., Wanke, E. 1996. A HERG-like K^+ channel in rat F-11 DRG cell line: pharmacological identification and biophysical characterization. *J. Physiol.* **496:**13–23
7. Gandhi, C. S., Clark, E., Loots, E., Pralle, A., Isacoff, E.Y. 2003. The orientation and molecular movement of a K^+ channel voltage-sensing domain. *Neuron* **40:**515–525
8. Gonzalez, C., Rosenman, E., Bezanilla, F., Alvarez, O., Latorre, R. 2001. Periodic perturbations in *Shaker* K^+ channel gating kinetics by deletions in the S3-S4 linker. *Proc. Natl. Acad. Sci. USA* **98:**9617–9623
9. Hidalgo, P., MacKinnon, R. 1995. Revealing the architecture of a K^+ channel pore through mutant cycles with a peptide inhibitor. *Science* **268:**307–310
10. Horn, R. 2004. How S4 segments move charge. Let me count the ways. *J. Gen. Physcol.* **123:**1–4
11. Jiang, Y., Lee, A., Chen, J., Cadene, M., Chait, B.T., MacKinnon, R. 2002. The open pore conformation of potassium channels. *Nature* **417:**523–526
12. Jiang, Y., Lee, A., Chen, J., Ruta, V., Cadene, M., Chait, B.T., MacKinnon, R. 2003. X-ray structure of a voltage-dependent K^+ channel. *Nature* **423:**33–41
13. Jiang, Y., Ruta, V., Chen, J., Lee, A., MacKinnon, R. 2003. The principle of gating charge movement in a voltage-dependent K^+ channel. *Nature* **423:**42–48
14. Kuo, A., Gulbis, J.M., Antcliff, J.F., Rahman, T., Lowe, E.D., Zimmer, J., Cuthbertson, J., Ashcroft, F.M., Ezaki, T., Doyle, D.A. 2003. Crystal structure of the potassium channel KirBac 1.1 in the closed state. *Science* **300:**1922–1926
15. Laine, M., Lin, M.-C.A., Bannister, J.P.A., Silverman, W.R., Mock, A.F., Roux, B., Papazian, D.M. 2003. Atomic proximity between S4 segment and pore domain in Shaker potassium channels. *Neuron* **39:**467–481
16. Lee, H.C., Wang, J.M., Swartz, K.J. 2003. Interaction between extracellular hanatoxin and the resting conformation of the voltage-sensor paddle in Kv channels. *Neuron* **40:**527–536
17. Li-Smerin, Y., Hackos, D.H., Swartz, K.J. 2000. α-Helical structure elements within the voltage-sensing domains of a K^+ channel. *J. Gen. Physiol.* **115:**33–49
18. Liu, J., Zhang, M., Jiang, M., Tseng., G.-N. 2003. Negative charges in the transmembrane domains of the HERG K channel are involved in the activation-and deactivation gating processes. *J Gen. Physol.* **121:**599–614
19. Long, S.B., Campbell, E.B., MacKinnon, R. 2005a. Crystal structure of a mammalian voltage-dependent *Shaker* family K^+ channel. *Science* **309:**897–903
20. Long, S.B., Campbell, E.B., MacKinnon, R. 2005b. Voltage sensor of Kv1.2: structural basis of electromechanical coupling. *Science* **309:**903–908
21. Lu, Y., Mahaut-Smith, M.P., Varghese, A., Huang, C.L.H., Kemp, P.R., Vandenberg, J.I. 2001. Effects of premature stimulation on HERG K^+ channels. *J. Physiol.* **537:**843–851
22. Mitcheson, J.S., Chen, J., Sanguinetti, M.C. 2000. Trapping of a methanesulfonanilide by closure of the HERG potassium channel activation gate. *J. Gen. Physio1.* **115:**229–239
23. Papazian, D. M., Silverman, W.R., Lin, M.-C.A., Tiwari-Woodruff, S.K., Tang, C.-Y. 2002. Structural organization of the voltage sensor in voltage-dependent potassium channels. *Novartis Foundation Symposium* **245:**178–192
24. Piper, D.R., Varghese, A., Sanguinetti, M.C., Tristani-Firouzi, M. 2003. Gating currents associated with intramembrane charge displacement in HERG potassium channels. *Proc. Natl. Acad. Sci. USA* **100:**10534–10539
25. Roden, D. M. 2004. Drug-induced prolongation of the QT interval. *N. Engl. J. Med.* **350:**1013–1022
26. Rosati, B., Marchetti, P., Crociani, O., Lecchi, M., Lupi, R., Arcangeli, A., Olivotto, M., Wanke, E. 2000. Glucose- and arginine-induced insulin secretion by human pancreatic (β-cells:the role of HERG K^+ channels in firing and release. *FASEB J.* **14:**2601–2610
27. Sanguinetti, M.C., Jiang, C., Curran, M.E., Keating, M.T. 1995. A mechanistic link between an inherited and an acquired cardiac arrhythmia: HERG encodes the I_{Kr} potassium channel. *Cell* **81:**299–307
28. Schreibmayer, W., Lester, H.A., Dascal, N. 1994. Voltage clamping of *Xenopus laevis* oocytes utilizing agarose-cushion electrodes. *Pfluegers Arch.* **426:**453–458
29. Shoeb, F., Malykhina, A.P., Akbarali, H.I. 2003. Cloning and functional characterization of the smooth muscle ether-a-go-go-related gene K^+ channel. *J. Biol. Chem.* **278:**2503–2514

30. Silverman, W.R., Roux, B., Papazian, D.M. 2003. Structural basis of two-stage voltage-dependent activation in K^+ channels. *Proc. Natl. Acad. Sci. USA* **100:**2935–2940
31. Smith P.L., Yellen G. 2002. Fast and slow voltage sensor movements in HERG potassium channels. *Gen. Physiol.* 119:275–293
32. Starace, D.M., Bezanilla, F. 2004. A proton pore in a potassium channel voltage sensor reveals a focused electric field. *Nature* **427:**548–553
33. Tiwari-Woodruff, S.K., Lin, M.-C.A., Schulteis, C.T., Papazian, D.M. 2000. Voltage-dependent structural interactions in the *Shaker* K^+ channel. *J. Gen. Physiol.* **115:**123–138
34. Tseng-Crank, J.C.L., Tseng, G.-N., Schwartz, A., Tanouye, M.A. 1990. Molecular cloning and functional expression of a potassium channel cDNA isolated from a rat cardiac library. *FEBS Lett.* **268:**63–68
35. Wang, S., Liu, S., Morales, M.J., Strauss, H.C., Rasmusson, R.L. 1997. A quantitative analysis of the activation and inactivation kinetics of *HERG* expressed in *Xenopus* oocytes. *J. Physiol.* **502:**45–60
36. Wang, X., Reynolds, E.R., Deak, P., Hall, L.M. 1997. The *seizure* locus encodes the *Drosophila* homolog of the HERG potassium channel. *J. Neurosci.* **17:**882–890
37. Yifrach, O., MacKinnon, R. 2002. Energetics of pore opening in a voltage-gated K^+ channel. *Cell* **111:**231–239
38. Zhang, M., Liu, J., Tseng, G.-N. 2004. Gating charges in the activation and inactivation processes of the hERG channel. *J. Gen.Physiol.* **124:**703–718
39. Zhou, W., Cayabyab, F.S., Pennefather, P.S., Schlichter, L.C., DeCoursey, T.E. 1998. HERG-like K^+ channels in microglia. *J. Gen. Physiol.* **111:**781–794